



From single crystal model catalysts to systematic studies of supported nanoparticles



Jozsef Speder^a, Ioannis Spanos^a, Alessandro Zana^a, Jacob J.K. Kirkensgaard^b, Kell Mortensen^b, Lena Altmann^{c,d}, Marcus Bäumer^{c,d}, Matthias Arenz^{a,*}

^a Nano-Science Center, Department of Chemistry, University of Copenhagen, Universitetsparken 5, DK-2100 Copenhagen Ø, Denmark

^b Niels Bohr Institute, University of Copenhagen, Universitetsparken 5, DK-2100 Copenhagen Ø, Denmark

^c Institute of Applied and Physical Chemistry, University of Bremen, Leobener Str. UFT, D-28359 Bremen, Germany

^d Center for Environmental Research and Sustainable Technology, University of Bremen, D-28359 Bremen, Germany

ARTICLE INFO

Available online 5 June 2014

Keywords:

Colloidal synthesis

Fuel cell catalysts

Oxygen reduction reaction

ABSTRACT

In the presented work we discuss our recent efforts to bridge the study of so-called model catalysts like well-defined single crystals and investigations of industrial catalysts, which are relatively ill-defined. Our work thereby concentrates on electrocatalytic processes that have relevance for low temperature fuel cells; mainly the oxygen reduction reaction and the stability of Pt based catalysts. Single crystal studies led to the development of many important concepts in this research field, but for example the stability of catalysts and mesoscopic effects like the particle proximity effect cannot be studied. Therefore we use a colloidal tool-box synthesis method, which allows systematic investigations on well-defined nano-structured, supported catalyst particles.

© 2014 Elsevier B.V. All rights reserved.

1. Introduction

A key issue in the catalytic research of proton exchange membrane (PEM) fuel cell catalysts is the relationship between nanoparticle structure, composition, support materials and catalytic activity. Over the years oxygen reduction reaction (ORR) activity studies by modern surface science techniques on well-oriented single crystal Pt surfaces have demonstrated the importance of surface structure for the mechanism and kinetics of this reaction [1–4]. Furthermore, bimetallic surfaces showed enhanced electrocatalytic reaction rates indicating the importance of ligand effects and/or strained crystal lattices [5–8]. This knowledge, which was mainly obtained by investigating model systems that are well defined and have reduced complexity in combination with theoretical studies has facilitated the development of industrial fuel cell catalysts and resulted in catalysts with improved catalytic activity [9].

Despite the success of single crystal studies, there is a need for studies with higher complexity that are more related to the catalytic systems used in fuel cells. In order to achieve high mass activities and to enhance the electrochemically accessible surface area (ECSA) in industrial catalysts, Pt nanoparticles (NPs) are usually dispersed on a support material [10]. The most widely used catalyst-supporting materials are high-

surface-area carbons (Ketjenblack EC-300 J, EC-600JD, Vulcan XC-72 and activated carbons). A wide range of physical and chemical methods has been developed to synthesize platinum nanoparticles. Amongst the chemical methods for the preparation of nanostructured catalysts, one of the most commonly applied methods is the impregnation–reduction method [11,12]. The principle of such methods involves the reduction of metallic precursor salts impregnating the carbon powder with either a reducing gas, sodium borohydride or by thermal treatment under inert atmosphere. Accordingly, the presence of active functional groups on the surface of the carbon powder plays a crucial role in the interaction between the catalyst precursor and support and therefore also in the obtained nanoparticle size and dispersion.

Considerable research has been devoted to transfer the knowledge obtained by single crystal studies to the nanoparticle level in such industrial catalysts [13–18]. In all these studies, however the systematic investigation of individual parameters, such as nanoparticle size or interparticle distance was limited by the fact that they were carried out on relatively poorly defined catalysts prepared by traditional synthesis routes (impregnation and precipitation methods). In such systems typically changing one parameter induces a change in related parameters. For instance, an increase in the metal weight loading results in an increase of the Pt NP size as well or a heating step to increase the Pt NP size also influences the support properties [19].

A more modern approach is to use colloidal synthesis to prepare catalysts. Colloidal methods have also been extensively used for the synthesis of platinum nanoparticles. Examples can be found using sodiumborohydride [20,21], sulfite-complex [22], water in oil microemulsion [23,24] and alcohol (or polyol) reduction based synthesis routes. These

* Corresponding author.

E-mail address: m.arenz@chem.ku.dk (M. Arenz).

methods have in common that they use various surfactants for stabilizing the colloidal suspension and controlling the particle size. As first introduced by Fievet et al. in the case of polyol methods, the metallic salt is reduced in the presence of polyol as a solvent by using its reducing and acid–base character/property that enables one to obtain a colloidal suspension of metallic nanoparticles protected by glycolate species [25,26]. Over the years a wide range of polyol based synthesis routes have been introduced, however the most commonly used and studied is the ethylene glycol based one [27–31].

In this case the metallic precursor ($\text{H}_2\text{PtCl}_6 \cdot 6\text{H}_2\text{O}$) is dissolved in an alkaline mixture solution of ethylene glycol and carbon powder ($\text{pH} = 11$) to create metal-oxides or -hydroxides. The dehydration reaction of ethylene glycol into acetaldehyde allows the reduction reaction of metal oxides or hydroxides. The metal seed growth process and final nanoparticle size is controlled by the adsorption of reaction by-products on the metal surface and the depletion of the metal salt to be reduced. Since the ethylene glycol creates a slow reaction path, the reaction is often activated either by temperature (at reflux, ca. 200 °C for 3 h) [32] or by microwave irradiation [29,33,34].

Another recently introduced synthesis method by Watanabe et al. relies on the simultaneous reduction of a mixture of $\text{Pt}(\text{acac})_2$, $\text{Fe}(\text{acac})_3$, ethylene glycol (as the solvent and reducing agent) and carbon black as the support. The reduction is achieved at 200 °C under N_2 atmosphere in reversed micelles. These reversed micelles act as nanoreactors, which enable to obtain particles with uniform size distribution due to the limited reaction space. After the reduction step, the organic moieties are removed from the metal surface by heat-treatment at 230 °C for 4 h in a flow of N_2 [35–37].

The above mentioned synthesis routes, i.e. impregnation and polyol methods, however have some disadvantages. First of all, the metal precursor salt may penetrate and be reduced in the pores of high surface area (HSA) carbons. As a consequence the metal NPs are later on not available for the electrochemical reaction, which decreases the maximum achievable ECSA. Another problem is that these methods often involve a high temperature heat treatment of the catalyst that changes the properties of the respective support [19,38]. For example, it has been shown that the platinum particles are able to catalyze the oxidation of a carbon support even at moderate temperatures (125–195 °C) [39]. The heat treatment therefore not only influences the carbon support itself, but it may also alter the initial Pt NP size and distribution by causing Pt sintering [40]. Finally, the limited flexibility of such synthesis routes inhibits systematic studies and especially the role of the substrate often is difficult to assess or impossible. It is also known that it is impossible to prepare highly loaded catalyst samples without causing the agglomeration of the NPs.

To bridge the gap between single-crystal model studies and studies of industrial catalysts we have recently introduced a new preparation method we dubbed tool-box approach [41]. In this approach carbon supported, Pt based catalysts are prepared from a colloidal suspension of well-defined Pt NPs synthesized by an ethylene-glycol (EG) method [32]. First, a mother solution of Pt NP in EG is prepared. The NPs are highly monodisperse and typically around 2 nm in diameter. In addition, the particles are free of any strongly binding surfactants or other agents and no heat treatment steps are required during synthesis. Using this approach, parameters such as support material, nanoparticle size and Pt to carbon ratio (interparticle distance between the NPs) can be uniquely tuned [41–43]. Therefore, the obtained electrocatalysts are ideally suitable for the examination of the influences of an individual parameter on the overall performance. This method offers new opportunities in the catalytic studies to investigate the detailed structural activity relationship at a nanoparticle level and to identify highly active and durable catalysts for the ORR.

In the present work we demonstrate the opportunities and challenges of our efforts to enable systematic studies on carbon supported NPs that serve as catalysts for low temperature fuel cells.

2. Experimental

2.1. Catalyst synthesis

The investigated catalysts, hereafter called Pt/C and PtCo/C, were synthesized in-house according to the ethylene glycol route described in Refs. [32,41]. The synthesis consists of two steps. First, a solution of colloidal Pt and PtCo NPs with narrow size distribution of around 2 nm is prepared, then the NPs are deposited in varying amounts onto the HSA carbon support, i.e. Ketjenblack EC-300 J (AkzoNobel, Brunauer-Emmett-Teller (BET) surface area: $795 \text{ m}^2 \text{ g}^{-1}$). Catalyst samples were prepared with various Pt loadings, between 10 and 80 wt.%. The actual Pt content of the catalysts was analyzed by ICP-MS (NexION 300X, Perkin Elmer) through a Meinhard quartz nebulizer and a cyclonic spray chamber, operating at nebulizer gas flow rates of between 1 and 1.02 l/min (Ar, purity 5.0). Before ICP analysis, the catalysts were dissolved in *aqua regia* (the volume ratio of HCl to HNO_3 was 3:1) and then diluted. The nominal and the actual Pt loading values agreed within 10–30%. As a general trend the difference decreased with higher loadings. For the calculation of the ECSA and the mass activities the actual Pt loading values were used.

2.2. Physical characterization

The electrocatalysts were characterized by Transmission Electron Microscopy (TEM) using a Tecnai T20 G2 (Philips FEI, Oregon, USA) equipped with a thermionic electron gun operated at 200 kV. The Platinum particle size distribution was determined by Small Angle X-ray Scattering (SAXS) using a SAXSLab instrument (JJ-Xray, Denmark). For more information, see Ref. [41].

2.3. Electrochemical characterization

The electrochemical measurements were performed using a computer controlled home-built potentiostat and a Teflon cell based on a three-compartment configuration using a rotating disk electrode (RDE) setup [44]. The counter (auxiliary) electrode was a platinum mesh, the reference electrode a Schott Ag/AgCl/KCl(sat) electrode placed in a separated compartment separated by an additional membrane (Nafion®) in order to avoid the diffusion of Cl^- ions into the main compartment [45]. All potentials in this work are referred to the reversible hydrogen electrode (RHE) potential, which was experimentally determined for each measurement series. All solutions were prepared in Millipore® water ($>18.3 \text{ M}\Omega \text{ cm}$, $\text{TOC} < 5 \text{ ppb}$). HClO_4 and HCl were from Merck (suprapur). The measurements were performed at 20 °C. Prior to the RDE measurements the glassy carbon (GC) working electrode (5 mm diameter, 0.196 cm^2 geometrical surface area) was polished to mirror finish using alumina oxide paste 0.3 and $0.05 \mu\text{m}$ (Buelher-Met, deagglomerated α -alumina and γ -alumina, respectively), and cleaned ultrasonically in ultrapure water and cc. 70% HClO_4 . The catalyst ink was prepared by ultrasonically dispersing the catalyst powder in ultrapure water ($0.14 \text{ mg}_{\text{Pt}} \text{ cm}^{-3}$). A volume of 20 μl of the suspension was then pipetted onto the GC electrode leading to a Pt loading of $14 \mu\text{g}_{\text{Pt}} \text{ cm}^{-2}$ and thereafter dried in a nitrogen gas stream. Only samples with a uniform catalyst film were analyzed. All electrochemical experiments were performed in 0.1 M HClO_4 solution. Prior to the measurements the electrolyte was de-aerated by purging with Ar gas (99.998%, Air Liquide), and the measurements were started with cleaning the catalyst by potential cycles between 0.05 and 1.1 V_{RHE} at a scan rate of 50 mV s^{-1} . The specific activity of the ORR was determined from the positive going RDE polarization curves recorded in O_2 saturated 0.1 M HClO_4 solution at a scan rate of 50 mV s^{-1} and at a rotation speed of 1600 rpm. In order to exclusively analyze the ORR current, the polarization curves were corrected for the non-faradaic background by subtracting the cyclic voltammograms recorded in Ar-purged electrolyte. Furthermore, the solution resistance between the

working electrode and the Luggin capillary was determined using an AC signal (5 kHz, 5 mV) and thereafter compensated for using the analog potentiostat's positive feedback scheme. The resulting effective solution resistance was less than 3 Ω in each experiment. The ECSA of the catalysts was determined from the CO stripping charge [46] recorded at a sweep rate of 50 mV s^{-1} . The mass activity was calculated based on the specific activity and the ECSA.

2.4. Calculation of the interparticle distance

As interparticle distance (*idp*) we define the average distance between the edge of a catalyst particle and the edge of its nearest neighboring catalyst particle given by [47]:

$$idp_{(edge\ to\ edge)} = \sqrt{\frac{A}{N}} - d_{NP}$$

where *A* is the BET surface area of support, *N* is the number of nanoparticles and *d_{NP}* is the average diameter of the nanoparticles, determined by TEM and SAXS. We assume for the calculation of the interparticle distance that all particles exhibit a spherical shape, the particles are monodispersed and homogeneously distributed on the carbon support. The theoretical interparticle distance is also compared with TEM micrographs.

3. Results and discussion

In order to overcome the discussed limitations in catalyst synthesis, in the tool-box preparation route [41] the synthesis of the Pt NPs and the supporting step on HSA carbons are separated, see scheme in Fig. 1. First, a solution of colloidal Pt NPs with narrow size distribution is prepared via an EG route [32]. Then, the NPs are precipitated from the EG-solution and resolved in acetone prior to deposition onto the HSA carbon support. The EG synthesis route allows the preparation of monodisperse NPs in the absence of strong binding organic stabilizing agents. The organic moieties are removed from NP surface by washing in HCl before attaching the NPs to the support. No temperature post-treatment of the catalyst is required rendering the approach ideally suitable for systematic catalytic studies.

3.1. Polyol synthesis as a toolbox for systematic model studies

In the following we demonstrate the flexibility and wide range of opportunities offered by this synthesis route for studying complex issues of PEM fuel cell reactions such as structure activity relationship and metal-support interaction. Recent examples include: the support variation and ionomer impregnation (a) and the metal loading variation (b). We investigated the influence of the support on the electrochemical properties of PEM fuel cell catalysts [41]. A series of catalysts based on the

same colloidal Pt NP suspension were synthesized, but with different HSA carbon supports and characterized by the RDE approach. As shown in Fig. 2, we found that the carbon support has no catalytic co-function for ORR activity in the prepared catalysts. However carbon pre-treatment, i.e. cc. HNO_3 treatment of the support may influence the apparent ECSA by enhancing the sticking of the Pt NPs on the support. It is shown that due to the reduced pinning of the support some of the NPs are lost in the synthesis. This leads to a mismatch between the expected and obtained Pt wt.% loading on the support. An unwanted side effect that occurs is NP agglomeration during synthesis. In Fig. 2 it is demonstrated that an enhanced NP sticking and a better NP dispersion without agglomeration can be accomplished by addition of nafion ionomer to the NP suspension [41].

Furthermore, the synthesis approach enables the flexible control of the Pt to carbon ratio in the prepared catalysts by mixing an appropriate amount of colloidal Pt NP suspension and carbon supports. The main advantage of the approach over conventional methods is that it enables the preparation of catalyst samples in a wide range of Pt wt.% without causing the agglomeration of the Pt NPs. To apply this tool in electrocatalytic model studies we have investigated the influence of Pt to C ration on the degradation behavior of prepared PEM fuel cell catalysts.

The degradation behavior was evaluated by measuring the change in ECSA under accelerated stress tests [42]. The degradation tests simulated load cycle (Fig. 3a) and start-up/shutdown conditions (Fig. 3b) and are adopted from Fuel Cell Commercialization Conference of Japan (FCCJ) recommendations [48]. As illustrated in Fig. 3a under conditions simulating the load cycle of PEM fuel cells no unambiguous correlation between the ECSA loss and the Pt:C ratio is found. However, under conditions simulating the repetitive start-up/shutdown processes of PEM fuel cells (Fig. 3b) the ECSA loss increases with increasing Pt loading. Such a trend could indicate the catalytic effect of Pt NPs on carbon corrosion, but Raman studies could not verify this hypothesis [49].

3.2. Combination of the particle proximity and metal alloying effects

One way to improve the cathode performance in PEM fuel cells is to use Pt that is alloyed with transition metals. It is known that Pt alloyed with Co, Cr, Cu and Ni enhances ORR activity as compared with pure Pt catalysts [5,8,50–56]. This phenomenon can be attributed to the fact that the second metal changes the atomic structure of the nanoparticles – by influencing the Pt–Pt interatomic distances, and/or changes the electronic structure of the Pt atoms – ligand effect [8,52,57].

Carbon-supported Pt-alloy based catalysts are conventionally prepared by the previously mentioned impregnation method where the second metal is simultaneously impregnated and deposited by the platinum precursor on the carbon support. This step then is followed by heating the catalyst at above 700 °C under an inert gas or hydrogen to form the alloy [50]. However, such a heat treatment often causes

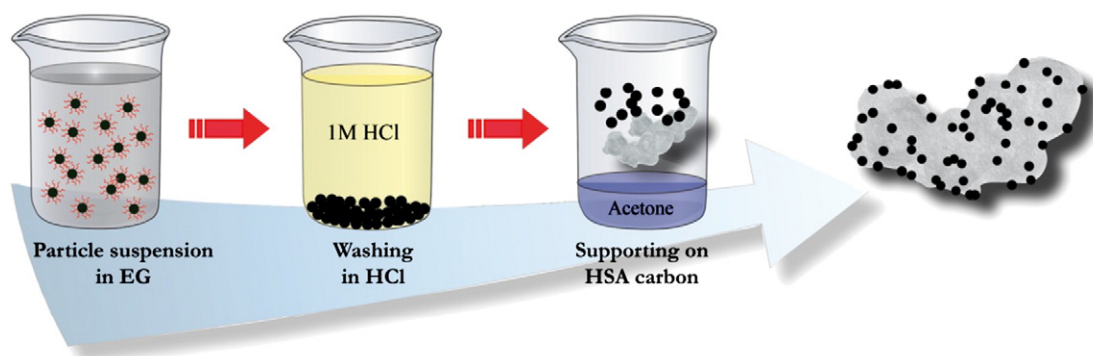


Fig. 1. Schematic of the EG method based PEM fuel cell catalyst preparation route. The red carbon tails indicate the protective function of the EG.

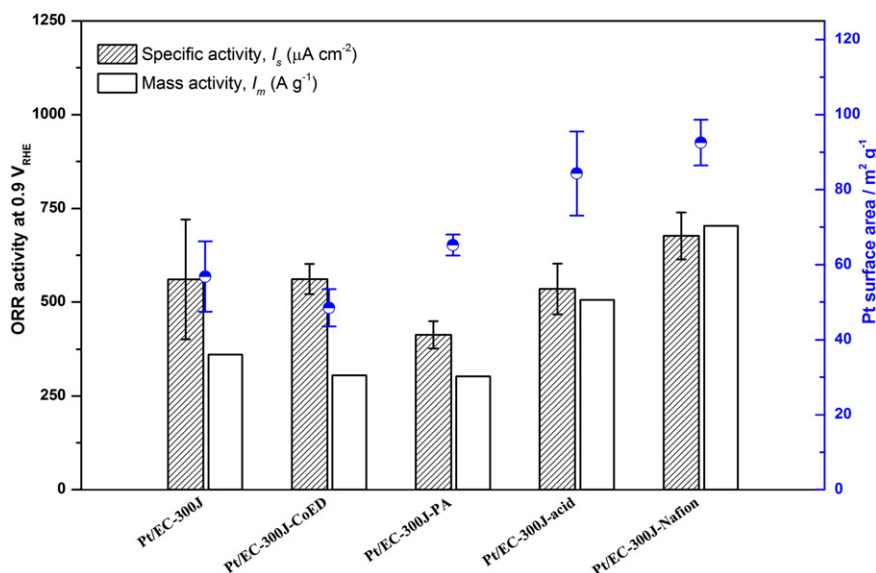


Fig. 2. Comparison of specific and mass activities of model catalysts for ORR measured in oxygen saturated 0.1 M HClO_4 at 0.9 V_{RHE} and room temperature. Pt surface areas (ECSAs) were determined from CO stripping. The mass activities were calculated from the respective specific activity and the ECSA [41].

metal particles sintering depending on the particle size. This results in a decrease of the Pt ECSA and an inherent loss of mass activity for the ORR.

The so-called colloid methods have also been widely used to prepare Pt-alloy bimetallic systems [58–60]. As reported by Santiago et al., by the application of long-chain diol (hexadecanediol), no heat treatment is necessary to form highly monodispersed PtCo nanoparticles with very small size and a high degree of alloying. However, even in such a synthesis method the PtCo NPs are deposited directly on the carbon support which limits the ability to flexibly control the composition of the prepared catalyst.

Recently, we started investigating a colloidal route using ethylene-glycol solution to produce PtCo NPs with narrow size distribution [61]. PtCo NPs are prepared by the method that is based on and the modification of the one developed by Wang et al. [32]. In order to investigate the combined effect of particle proximity and metal alloying, we have prepared Pt and PtCo (1:1) catalysts with varying Pt loading between 20 and 80 wt.% on Ketjenblack EC-300 J. As previously demonstrated $\text{Pt}_x\text{Co}_{1-x}$ catalysts are not stable under acidic conditions and the less

noble component (Co) is leached out when in contact with the electrolyte [54,62]. In the case of the EG route, the use of 1 M HCl for washing the NPs does not only result in the removal of ethylene-glycol residues, but also the chemical dissolution of the cobalt. Therefore, after supporting the PtCo NPs onto the carbon support the particles can be dubbed $\text{Pt}_x\text{Co}_{1-x}$ skeleton NPs. Furthermore, when the catalyst samples are subjected to the electrolyte in RDE measurements a spontaneous electrochemical leaching occurs. In order to see the impact of the acid leaching on the metal content the catalyst samples were dissolved in *aqua regia* and analyzed by ICP-MS. The analysis of ICP-MS measurement confirmed that acid leaching leads to a severe change in composition of the PtCo skeleton NPs, i.e. from the initial 50 at.% the Co content is reduced to about 2.5–4.5 at.%. Furthermore, the Pt content of the prepared samples was also determined in order to see the amount of Pt NPs that is attached to the carbon surface during the catalyst preparation. Based on the analysis, the difference between experimental and nominal Pt content was between 10 and 25% in all samples (the lower values were obtained for high Pt loading).

Examples of TEM micrographs of the 30 wt.% Pt/C and PtCo/C catalysts are shown in Fig. 4. The micrographs reveal that the Pt and PtCo NPs are well dispersed on the carbon support and that there is no or only small nanoparticle agglomeration. In order to gain a better overview and to confirm the particle size distribution small angle X-ray scattering measurements were performed. The results of the NP size analysis of the Pt/C and PtCo/C catalysts with 30 wt.% Pt loading are shown in the insets of Fig. 4. In agreement with the TEM micrographs, SAXS reveals well-dispersed NPs with an average diameter of ca. 2 nm. For the 30 wt.% Pt and the acid leached PtCo/C samples the estimated average particle diameter is 2.20 ± 1.32 nm (FWHM as error) and 2.16 ± 1.12 nm, respectively.

In Fig. 5 the ECSA values of the Pt/C and pre-leached PtCo/C samples are summarized as a function of the nominal Pt loading ranging between 20 and 80 Pt wt.%. As seen the ECSA varies between 75 and $80 \text{ m}^2 \text{g}^{-1}$ for Pt/C while for the PtCo/C samples values between 50 and $85 \text{ m}^2 \text{g}^{-1}$ were obtained. Pt NPs can be supported on the HSA carbon up to extremely high loadings of 80 Pt wt.% without ECSA loss, whereas the ECSA of the pre-leached PtCo/C apparently continuously decreases with increasing Pt loading. Thus the data indicate that the agglomeration of the PtCo NPs on the carbon support starts at a lower Pt loading as compared to pure Pt NPs. Most likely the agglomeration already occurs during the supporting step and not during the electrochemical measurements as the samples were not subjected to

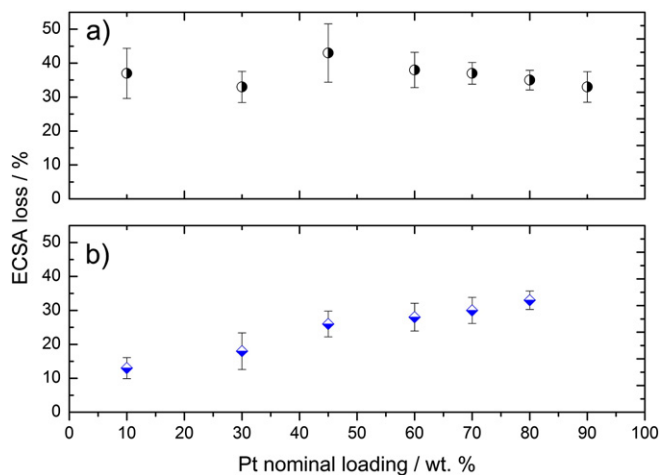


Fig. 3. Summary of the determined ECSA loss for Pt/Ketjenblack EC 300 J as function of Pt loading. In a) the catalysts were subjected to potential steps between 0.6 and 1.0 V_{RHE} with a holding time of 3:3 s (simulating load cycles) for 9000 cycles. In b) the catalysts were treated by potential cycling between 1.0 and 1.5 V_{RHE} with a sweep rate of 500 mV s^{-1} (simulating Start-Stop cycles) for 27,000 cycles. All measurements were conducted in 0.1 M HClO_4 electrolyte and at room temperature [42].

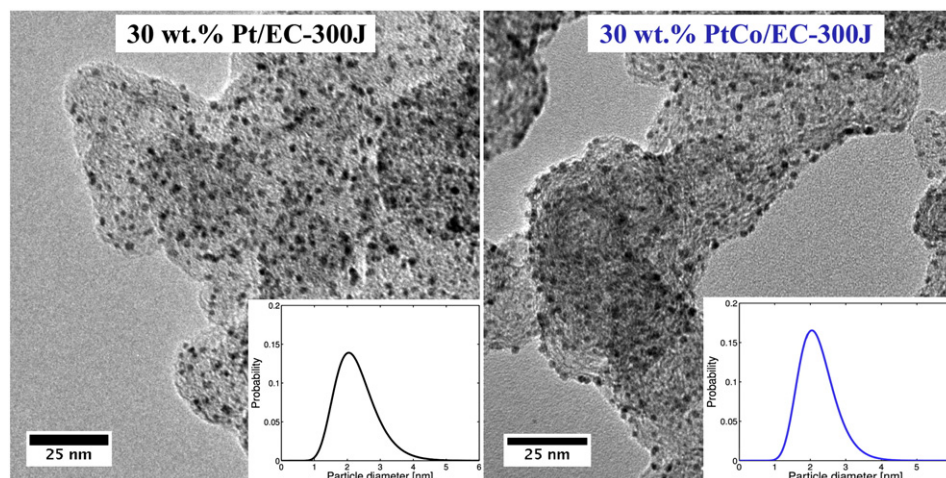


Fig. 4. TEM micrographs of the synthesized catalysts for 30 wt.% Pt/C (left hand side) and PtCo/C (right hand side) catalysts. The insets show the particle size (diameter) distribution of the catalysts as determined in SAXS.

excessive potential cycling. This means that the particle sticking of the PtCo NPs to the support is lower as compared to the Pt NPs.

Such agglomeration has considerable consequences on the electrocatalytic performance of the NPs. The ORR activity of the Pt/C and pre-leached PtCo/C catalysts was determined using the RDE thin film approach [63,64]. The ORR activity of the catalysts is characterized by the surface area specific turnover rate measured at $0.9 V_{\text{RHE}}$, the so-called specific activity (SA). Fig. 6 summarizes the surface specific activity of the Pt/C and the pre-leached PtCo/C samples as a function of the nominal Pt weight loading. As can be seen, there is a strong correlation between the ORR activity and the metal loading. With increasing Pt weight loading the SA increases from 470 to $775 \mu\text{A cm}^{-2}$ in the case of Pt/C and from 670 to $1280 \mu\text{A cm}^{-2}$ in the case of PtCo/C, respectively.

As we have previously reported, on Pt cluster model systems a correlation between the SA and the average distance between neighboring particles was found, i.e. the particle proximity effect [47]. It was observed that the SA increases in a nonlinear fashion as more and more Pt clusters were deposited, independent of their size. Normalization of the activity values to the interparticle distance led to a unified trend in SA increase. Significantly improved SA can, however, only be observed at extremely small interparticle distances, i.e. shortly before the clusters agglomerate. While a conclusive model for this mesoscopic effect is still lacking, our hypothesis is that the reduced interparticle distance leads to a change in the properties of the electric double layer [47].

Transferring the study of the Pt cluster model systems to applied catalysts is an important step for the verification of the discussed particle proximity phenomenon [65]. On carbon supported catalysts the interparticle distance can be easily correlated to the Pt loading. Thus the effect observed in this work can at least in part be assigned to the same phenomenon; for Pt/C the increase in Pt loading at constant ECSA correlates to a decreased interparticle distance, which results in a higher SA. For PtCo/C the situation is more complex. At low and intermediate Pt loading the obtained SA of pre-leached PtCo/C is ca. 25–30% higher than those obtained with the corresponding Pt/C samples. This activity enhancement has been previously studied and mainly be assigned to a strain effect of the leached PtCo NPs [8,62,66]. At high Pt loadings, i.e. 70 and 80 wt.% Pt, the difference between Pt/C and PtCo/C, however, increases. At the same time for these two samples the ECSA values indicate NP agglomeration (see Fig. 5). Therefore in these samples the particle proximity effect is overlapped with a particle size effect [13,17,67–69], both contributing to a SA increase.

From the SA and the ECSA, the mass specific activity (MA) can be calculated. The MA is a widely used parameter to compare PEM fuel cell electrocatalysts from an economical, cost effective point of view. The calculated MAs are displayed in Fig. 7. In the case of the Pt/C samples the MA increases with increasing Pt loading from 350 to 625 A g^{-1} . In other words by increasing the loading and thereby decreasing the interparticle distance the efficiency of the catalyst can be almost doubled. By

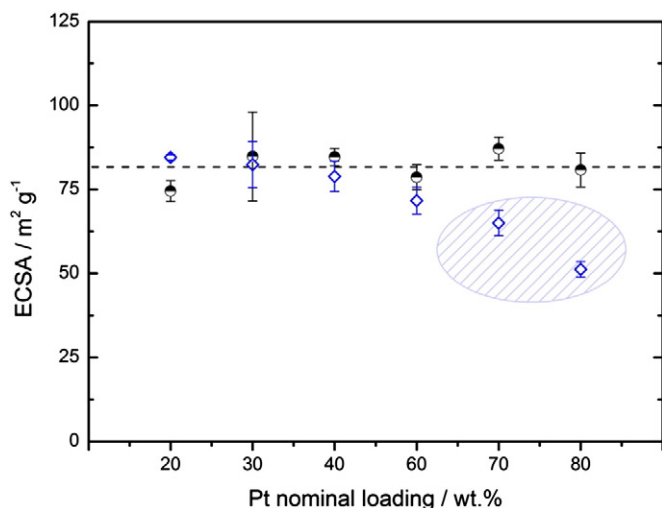


Fig. 5. ECSA of the Pt/C and PtCo/C catalyst samples as a function of the nominal catalyst loading in Pt wt.%. The shaded area indicates particle agglomeration.

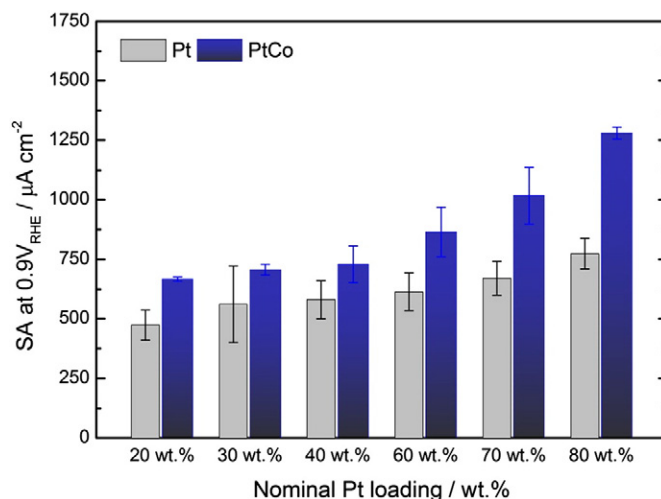


Fig. 6. Comparison of specific activities (SA) of Pt/C and PtCo/C catalysts for ORR measured in oxygen saturated 0.1 M HClO_4 at $0.9 V_{\text{RHE}}$ and room temperature.

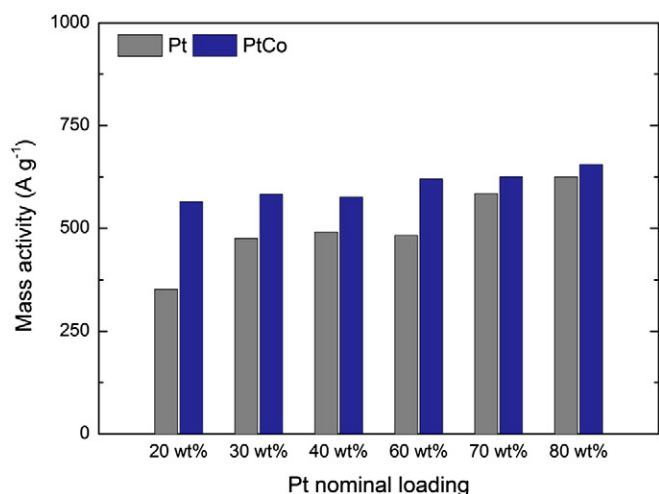


Fig. 7. Comparison of mass activities of Pt/C and PtCo/C catalysts for ORR measured in oxygen saturated 0.1 M HClO₄ at 0.9 V_{RHE} and room temperature.

contrast for PtCo/C the MA is almost constant, irrespective of the Pt nominal wt.%. Increasing the Pt loading from 20 to 80 wt.%, the MA only increases from 575 to 650 A g⁻¹. This result clearly demonstrates that the MA only can be optimized if particle agglomeration can be avoided and the ECSA remains sufficiently high as is the case for the Pt/C, but not the PtCo/C samples. As a consequence the maximum MA of Pt/C is almost the same as the maximum MA of PtCo/C. At this point it is not clear what effect causes the PtCo agglomeration during synthesis and further studies are necessary to suppress this unwanted effect.

Discussing the particle proximity effect, i.e. the influence of the interparticle distance on the catalytic activity, it is instructive to analyze the cyclic voltammograms of the different catalysts. In literature, the peak potential of Pt oxide reduction in a cyclic voltammograms is often correlated with the catalytic activity for the ORR [70,71]. It is assumed that depending on their adsorption strength on Pt, OH-species act as reaction intermediate or as blocking species inhibiting the ORR. In order to elucidate if the catalytic activity can be linked to the Pt oxide reduction peak of our catalysts, we investigated the cyclic voltammograms and analyzed the Pt oxide reduction peak position. The results are displayed in Fig. 8, where we plotted the peak potential of the Pt oxide reduction peak as a function of the interparticle distance. The peak potential of oxide reduction on polycrystalline Pt serves as

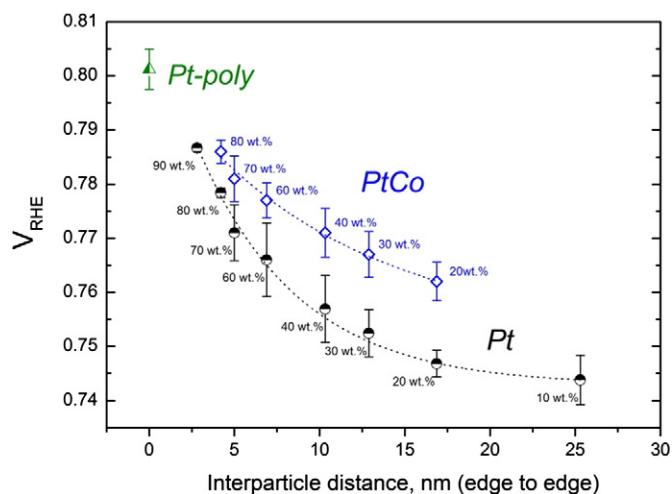


Fig. 8. Oxygen reduction peak potentials for Pt/C and PtCo/C samples as a function of the estimated interparticle distance (edge to edge) measured in 0.1 M HClO₄ with a sweep rate of 50 mV s⁻¹ at room temperature. For PtCo the estimation of the interparticle distance did not take Co leaching into account.

benchmark. The peak potential of the oxide reduction varies between 0.745 and 0.805 V_{RHE} with the 10 wt.% Pt/C sample having the lowest peak potential and polycrystalline Pt the highest. It should be also noticed that the PtCo/C samples have relatively higher peak potential values as compared to the Pt/C samples. Moreover, there is a distinct shift in the peak potential to a higher potential as the interparticle distance decreases. These observations thus confirm the correlation between the OH adsorption strength and the ORR activity.

4. Conclusions

In order to bridge the gap between single-crystal model studies and studies of industrial catalysts, synthesis approaches are needed that deliver well-defined nanoparticles attached to high surface area supports. Furthermore the ability to individually change one parameter such as the interparticle distance without influencing other parameters such as the particle size is essential to unravel trends such as the particle proximity effect.

The approach we pursue is based on a two-step process. First a colloidal suspension of well-defined Pt NPs is synthesized and in a second step the NPs are supported on a high surface area substrate. Our results indicate that changing the interparticle distance the OH adsorption strength on the NPs can be optimized in a similar fashion as by alloying Pt with another metal. Using pure Pt NPs, the observed weakening of the OH adsorption strength is genuinely ascribed to the particle proximity effect, whereas for PtCo NP agglomeration is observed. This inhibits a distinction between a particle size and the particle proximity effect.

Acknowledgments

This work was supported by the Danish DFF through grant no. 10-081337 and the European Cost Action MP0903 Nanoalloys. We acknowledge Andrea Mingers of the group of Dr. Karl J.J. Mayrhofer at the MPIE for the ICP-MS analysis.

References

- [1] J. Snyder, N. Danilovic, A.P. Paulikas, D. Tripkovic, D. Strmcnik, N.M. Markovic, V.R. Stamenkovic, *J. Phys. Chem. C* 117 (2013) 23790.
- [2] N.M. Marković, R.R. Adžić, B.D. Cahan, E.B. Yeager, *J. Electroanal. Chem.* 377 (1994) 249.
- [3] N.M. Markovic, H.A. Gasteiger, P.N. Ross, *J. Phys. Chem.* 99 (1995) 3411.
- [4] M.D. Maciá, J.M. Campiña, E. Herrero, J.M. Feliu, *J. Electroanal. Chem.* 564 (2004) 141.
- [5] J. Greeley, I.E.L. Stephens, A.S. Bondarenko, T.P. Johansson, H.A. Hansen, T.F. Jaramillo, J. Rossmeisl, I. Chorkendorff, J.K. Nørskov, *Nat. Chem.* 1 (2009) 552.
- [6] V. Stamenkovic, T.J. Schmidt, P.N. Ross, N.M. Markovic, *J. Phys. Chem. B* 106 (2002) 11970.
- [7] V.R. Stamenkovic, B. Fowler, B.S. Mun, G. Wang, P.N. Ross, C.A. Lucas, N.M. Markovic, *Science* 315 (2007) 493.
- [8] P. Strasser, et al., *Nat. Chem.* 2 (2010) 454.
- [9] J.K. Nørskov, T. Bligaard, J. Rossmeisl, C.H. Christensen, *Nat. Chem.* 1 (2009) 37.
- [10] M.S. Wilson, S. Gottesfeld, *J. Appl. Electrochem.* 22 (1992) 1.
- [11] A.S. Aricò, Z. Poltarzewski, H. Kim, A. Morana, N. Giordano, V. Antonucci, *J. Power Sources* 55 (1995) 159.
- [12] T. Kawaguchi, W. Sugimoto, Y. Murakami, Y. Takasu, *J. Catal.* 229 (2005) 176.
- [13] K.J.J. Mayrhofer, B.B. Blizanac, M. Arenz, V.R. Stamenkovic, P.N. Ross, N.M. Markovic, *J. Phys. Chem. B* 109 (2005) 14433.
- [14] K. Kinoshita, *J. Electrochem. Soc.* 137 (1990) 845.
- [15] M. Watanabe, H. Sei, P. Stonehart, *J. Electroanal. Chem.* 261 (1989) 375.
- [16] K.J.J. Mayrhofer, D. Strmcnik, B.B. Blizanac, V. Stamenkovic, M. Arenz, N.M. Markovic, *Electrochim. Acta* 53 (2008) 3181.
- [17] M. Nesselberger, S. Ashton, J.C. Meier, I. Katsounaros, K.J.J. Mayrhofer, M. Arenz, *J. Am. Chem. Soc.* 133 (2011) 17428.
- [18] M. Uchida, Y. Fukuoka, Y. Sugawara, N. Eda, A. Ohta, *J. Electrochem. Soc.* 143 (1996) 2245.
- [19] K. Schlögl, M. Hanziik, M. Arenz, *J. Electrochem. Soc.* 159 (2012) B677.
- [20] H. Bönnemann, W. Brijoux, R. Brinkmann, T. Joußen, B. Korall, E. Dinjus, *Angew. Chem. Int. Ed. Engl.* 30 (1991) 1312.
- [21] H. Bönnemann, W. Brijoux, R. Brinkmann, R. Fretzen, T. Jousen, R. Köppler, B. Korall, P. Neiteler, *J. Richter, J. Mol. Catal.* 86 (1994) 129.
- [22] M. Watanabe, M. Uchida, S. Motoo, *J. Electroanal. Chem. Interfacial Electrochem.* 229 (1987) 395.
- [23] M. Boutonnet, J. Kizling, P. Stenius, G. Maire, *Colloids Surf.* 5 (1982) 209.
- [24] S. Brimaud, C. Coutanceau, E. Garnier, J.M. Léger, F. Gérard, S. Pronier, M. Leoni, *J. Electroanal. Chem.* 602 (2007) 226.
- [25] F. Fievet, J.P. Lagier, M. Figlarz, *MRS Bull.* 14 (1989) 29.

- [26] F. Fievet, J.P. Lagier, B. Blin, B. Beaudoin, M. Figlarz, *Solid State Ionics* 32–33 (Part 1) (1989) 198.
- [27] D. Larcher, R. Patrice, *J. Solid State Chem.* 154 (2000) 405.
- [28] X. Yan, H. Liu, K.Y. Liew, *J. Mater. Chem.* 11 (2001) 3387.
- [29] Z. Liu, J.Y. Lee, W. Chen, M. Han, L.M. Gan, *Langmuir* 20 (2003) 181.
- [30] F. Bonet, V. Delmas, S. Grugeon, R. Herrera Urbina, P.Y. Silvert, K. Tekaiia-Elhissien, *Nanostruct. Mater.* 11 (1999) 1277.
- [31] T. Herricks, J. Chen, Y. Xia, *Nano Lett.* 4 (2004) 2367.
- [32] Y. Wang, J.W. Ren, K. Deng, L.L. Gui, Y.Q. Tang, *Chem. Mater.* 12 (2000) 1622.
- [33] S. Song, Y. Wang, P.K. Shen, *J. Power Sources* 170 (2007) 46.
- [34] S. Komarneni, D. Li, B. Newalkar, H. Katsuki, A.S. Bhalla, *Langmuir* 18 (2002) 5959.
- [35] H. Yano, M. Kataoka, H. Yamashita, H. Uchida, M. Watanabe, *Langmuir* 23 (2007) 6438.
- [36] M. Uchida, Y.-C. Park, K. Kakinuma, H. Yano, D.A. Tryk, T. Kamino, H. Uchida, M. Watanabe, *Phys. Chem. Chem. Phys.* 15 (2013) 11236.
- [37] H. Yano, E. Higuchi, H. Uchida, M. Watanabe, *J. Phys. Chem. B* 110 (2006) 16544.
- [38] S.J. Ashton, M. Arenz, *Electrochem. Commun.* 13 (2011) 1473.
- [39] D.A. Stevens, J.R. Dahn, *Carbon* 43 (2005) 179.
- [40] P.C. Flynn, S.E. Wanke, *J. Catal.* 37 (1975) 432.
- [41] J. Speder, L. Altmann, M. Roefzaad, M. Bäumer, J.J.K. Kirkensgaard, K. Mortensen, M. Arenz, *Phys. Chem. Chem. Phys.* 15 (2013) 3602.
- [42] J. Speder, A. Zana, I. Spanos, J.J.K. Kirkensgaard, K. Mortensen, M. Arenz, *Electrochem. Commun.* 34 (2013) 153.
- [43] J. Speder, L. Altmann, M. Bäumer, J.J.K. Kirkensgaard, K. Mortensen, M. Arenz, *RSC Adv.* 4 (29) (2014) 14971–14978.
- [44] K.J.J. Mayrhofer, G.K.H. Wiberg, M. Arenz, *J. Electrochem. Soc.* 155 (2008) P1.
- [45] K.J.J. Mayrhofer, S.J. Ashton, J. Kreuzer, M. Arenz, *Int. J. Electrochem. Sci.* 4 (2009) 1.
- [46] H.A. Gasteiger, N. Markovic, P.N. Ross, E.J. Cairns, *J. Phys. Chem.* 98 (1994) 617.
- [47] M. Nesselberger, et al., *Nat. Mater.* 12 (2013) 919.
- [48] A. Ohma, K. Shinohara, A. Iiyama, T. Yoshida, A. Daimaru, in: H.A. Gasteiger, et al., (Eds.), *Polymer Electrolyte Fuel Cells*, 11, 2011, p. 775.
- [49] A. Zana, J. Speder, N.E.A. Reeler, T. Vosch, M. Arenz, *Electrochim. Acta* 114 (2013) 455.
- [50] L. Xiong, A. Manthiram, *J. Electrochem. Soc.* 152 (2005) A697.
- [51] E. Antolini, *Appl. Catal. B Environ.* 74 (2007) 324.
- [52] S. Mukerjee, S. Srinivasan, M.P. Soriaga, J. McBreen, *J. Phys. Chem.* 99 (1995) 4577.
- [53] V. Stamenkovic, B.S. Mun, K.J.J. Mayrhofer, P.N. Ross, N.M. Markovic, J. Rossmeisl, J. Greeley, J.K. Nørskov, *Angew. Chem. Int. Ed.* 45 (2006) 2897.
- [54] V.R. Stamenkovic, B.S. Mun, M. Arenz, K.J.J. Mayrhofer, C.A. Lucas, G. Wang, P.N. Ross, N.M. Markovic, *Nat. Mater.* 6 (2007) 241.
- [55] C.H. Cui, L. Gan, M. Heggen, S. Rudi, P. Strasser, *Nat. Mater.* 12 (2013) 765.
- [56] D.F. van der Vliet, C. Wang, D. Tripkovic, D. Strmcnik, X.F. Zhang, M.K. Debe, R.T. Atanasoski, N.M. Markovic, V.R. Stamenkovic, *Nat. Mater.* 11 (2012) 1051.
- [57] M.-k. Min, J. Cho, K. Cho, H. Kim, *Electrochim. Acta* 45 (2000) 4211.
- [58] W. Li, W. Zhou, H. Li, Z. Zhou, B. Zhou, G. Sun, Q. Xin, *Electrochim. Acta* 49 (2004) 1045.
- [59] E.I. Santiago, L.C. Varanda, H.M. Villullas, *J. Phys. Chem. C* 111 (2007) 3146.
- [60] N. Toshima, Y. Wang, *Langmuir* 10 (1994) 4574.
- [61] I. Spanos, C.P. Rellán, L. Altmann, M. Bäumer, M. Arenz, *Int. J. Hydrog. Energy* 39 (2014) 9143.
- [62] I. Spanos, J.J.K. Kirkensgaard, K. Mortensen, M. Arenz, *J. Power Sources* 245 (2014) 908.
- [63] T.J. Schmidt, H.A. Gasteiger, G.D. Stab, P.M. Urban, D.M. Kolb, R.J. Behm, *J. Electrochem. Soc.* 145 (1998) 2354.
- [64] U.A. Paulus, T.J. Schmidt, H.A. Gasteiger, R.J. Behm, *J. Electroanal. Chem.* 495 (2001) 134.
- [65] J. Speder, L. Altmann, M. Bäumer, J.J.K. Kirkensgaard, K. Mortensen, M. Arenz, *Rsc Adv.* 4 (2014) 14971.
- [66] I.E.L. Stephens, A.S. Bondarenko, U. Gronbjerg, J. Rossmeisl, I. Chorkendorff, *Energy Environ. Sci.* 5 (2012) 6744.
- [67] H.A. Gasteiger, S.S. Kocha, B. Sompalli, F.T. Wagner, *Appl. Catal. B Environ.* 56 (2005) 9.
- [68] M. Arenz, K.J.J. Mayrhofer, V. Stamenkovic, B.B. Blizanac, T. Tomoyuki, P.N. Ross, N.M. Markovic, *J. Am. Chem. Soc.* 127 (2005) 6819.
- [69] F.J. Perez-Alonso, D.N. McCarthy, A. Nierhoff, P. Hernandez-Fernandez, C. Streb, I.E.L. Stephens, J.H. Nielsen, I. Chorkendorff, *Angew. Chem. Int. Ed.* 51 (2012) 4641.
- [70] P.J. Ferreira, G.J. la O, Y. Shao-Horn, D. Morgan, R. Makharia, S. Kocha, H.A. Gasteiger, *J. Electrochem. Soc.* 152 (2005) A2256.
- [71] N.M. Marković, T.J. Schmidt, V. Stamenković, P.N. Ross, *Fuel Cells* 1 (2001) 105.